Extended quantum Maxwell demon acting over macroscopic distances

A. V. Lebedev,[1,2] G. B. Lesovik,[1] V. M. Vinokur,[3] and G. Blatter[2]

[1]*Moscow Institute of Physics and Technology, Institutskii per. 9, Dolgoprudny, 141700, Moscow District, Russia*
[2]*Theoretische Physik, Wolfgang-Pauli-Strasse 27, ETH Zurich, CH-8093 Zürich, Switzerland*
[3]*Materials Science Division, Argonne National Laboratory, 9700 South Cass Avenue, Argonne, Illinois 60439, USA*

A quantum Maxwell demon is a device that can lower the entropy of a quantum system by providing it with purity. The functionality of such a quantum demon is rooted in a quantum-mechanical SWAP operation exchanging mixed and pure states. We describe the setup and performance of a quantum Maxwell demon that purifies an energy-isolated system from a distance. Our cQED-based design involves two transmon qubits, where the mixed-state target qubit is purified by a pure-state demon qubit connected via an off-resonant transmission line; this configuration naturally generates an iSWAP gate. Although less powerful than a full SWAP gate, we show that assuming the present-day performance characteristics of a cQED implementation, such an extended quantum Maxwell demon can purify the target qubit over macroscopic distances on the order of meters and tolerates elevated temperatures of the order of a few Kelvin in the transmission line.

I. INTRODUCTION

Maxwell's demon [1] is a putative device that is capable of observing and controlling the microscopic degrees of freedom of a thermodynamic system. The existence of such a demon permits the cyclic extraction of work in a heat engine with unit efficiency and thus apparently violates the second law of thermodynamics. After a century-long debate [2], it has been realized by Landauer [3] and by Bennett [4] that the demon's functionality requires a memory in which to store the results of its observations. The cyclic operation of the engine then must include an element that erases the information in the demon's memory. According to Landauer, this erasure involves an entropy increase per bit of $\Delta S = k_B \ln 2$. A crucial element in furthering the argument is to include the demon, which is situated in the immediate proximity of the system, as a part of the system. As a natural consequence, the thermodynamic cost of erasing the demon's memory then is accounted for in the engine's overall entropy budget, thereby restoring the validity of the second law. Thermodynamic machines utilizing the functionality of such a locally operating classical Maxwell demon have been recently demonstrated in several systems [5–8].

Within a quantum-mechanical framework, new opportunities arise, e.g., a demon has been conceived [9] that enables the entropy of an energy-isolated system to be reduced. This has inspired the proposal for an engine that features separated cycles [10,11], an energy cycle that transforms heat into work without thermal waste, and an entropy cycle that restores the second law. These findings motivate the question about the distance over which such a quantum Maxwell demon can perform its beneficial action. In this paper, we analyze the performance of an extended quantum Maxwell demon (QMD); specifically, we determine the demon's maximal spatial separation and its operating conditions that allow for an entropy reduction of a distant energy-isolated quantum system. This removes the question about a possible local violation of the second law to a quantitative level. Furthermore, such a separation between the system and the demon is of practical relevance as it naturally protects the system against undesired heating during the demon's Landauer purification; within the context of quantum information processing, an extended demon can be used to feed pure states to an ongoing quantum computation. In a wider context, the coherent communication between quantum systems separated by large distances [12,13] is of great relevance, e.g., in distant entanglement [14], in recent Bell tests [15,16], and in quantum state transfer [17].

A first version of a quantum Maxwell demon has been proposed by Lloyd [18] in the context of nuclear magnetic resonance experiments (see also Refs. [19–21]), based on the idea that such a device exchanges the mixed quantum state of a *target* system with a purer quantum state of the *demon*. Such an exchange is realized in the course of the coherent unitary evolution of the joint target-demon system. In contrast to the classical version, the quantum demon utilizes its quantum purity as a thermodynamic resource and does not measure the state of the target system, hence its functionality is rooted in purity rather than information [22]. Several proposals for QMD-assisted thermodynamic machines have been suggested [10,23–27], but only a few have been realized experimentally [28–30]. Here, we describe a practical design of a spatially distributed QMD setup that is able to purify the state of a distant quantum system, the target qubit, by deterministically transforming its unknown mixed state into a given pure quantum state that is provided by the demon.

Below, we focus on a circuit QED implementation with two distant transmon qubits [31], namely the target and the demon qubits, that are capacitively coupled via a bosonic bath in the form of a transmission line [32]; see Fig. 1. This setup leads to an XY-type interaction between the qubits that naturally generates an iSWAP gate—the latter's purification power is reduced as compared to a full SWAP gate.
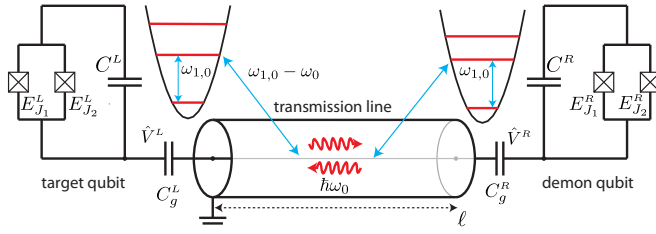
FIG. 1. Schematic setup for an extended quantum Maxwell demon swapping the mixed state of the target qubit (left) with the pure state of the demon qubit (right) via an autonomous and energy-conserving process. The qubits are formed by the two low-energy states of a transmon device comprised of a SQUID loop with two Josephson junctions with energies $E_{J_1}^{\alpha}$ and $E_{J_2}^{\alpha}$, capacitively shunted by a large capacitor C^{α} ($\alpha = $ L,R); for the transmon, $E_C^{\alpha} = e^2/2C^{\alpha} \ll E_{J_{1,2}}^{\alpha}$. The off-resonant transmission line of length ℓ connecting the two qubits is filtered to a frequency band $\Delta\omega$ around ω_0 and generates an XY-type interaction that remains effective at macroscopic distances ℓ and elevated temperature $T_{\text{line}} \gg T_{\text{qubit}}$.

However, the simpler implementation and enhanced robustness to decoherence of the iSWAP gate motivate us to focus on this simpler version of a quantum demon in our analysis below. We then address two main questions: (i) what spatial separation between target and demon qubits can be achieved for such an extended quantum demon, given the finite coherence time of the components, and (ii) what are the requirements for the thermodynamic state of the bosonic bath, the transmission line, that mediates the interaction between the systems. We find that, given typical parameters describing present-day cQED systems, a distance ℓ of the order of a few meters can be reached with a transmission line operating in the Kelvin range, i.e., about two orders of magnitude higher than the operating temperature of the qubits.

II. cQED SETUP OF AN EXTENDED QUANTUM DEMON

A target-demon setup of the type outlined above is described by the Hamiltonian

$$\hat{H} = \sum_{\alpha=\text{L,R}} \sum_{i=0}^{\infty} \epsilon_i^{\alpha} |i\rangle_{\alpha}{}_{\alpha}\langle i| + \hat{H}_{\text{line}}$$

$$+ \sum_{\alpha=\text{L,R}} \sum_{i=0}^{\infty} [q_{i+1,i}^{\alpha} \hat{V}^{\alpha}(x^{\alpha}) |i+1\rangle_{\alpha}{}_{\alpha}\langle i| + \text{H.c.}], \quad (1)$$

where ϵ_i^{α} and $|i\rangle_{\alpha}$ describe the energy levels of the left and right ($\alpha = $ L, R) transmon qubits positioned at $x^{\text{L}} = -\ell/2$ and $x^{\text{R}} = +\ell/2$, and $\hat{V}(x)$ is the voltage at position x along the transmission line. The latter generates an additional voltage drop $\beta^{\alpha} \hat{V}^{\alpha}(x^{\alpha})$ across the qubit capacitor, where the reduction factors $\beta^{\alpha} = C_g^{\alpha}/(C_g^{\alpha} + C^{\alpha})$ account for the capacitors' geometries; see Fig. 1. This voltage drop couples to the Cooper pairs $\hat{n}^{\alpha}$ transferred between the transmon capacitor with the effective charge $q_{i+1,i}^{\alpha} = 2e\,\beta^{\alpha}{}_{\alpha}\langle i + 1|\hat{n}^{\alpha}|i\rangle_{\alpha}$, where we incorporate the geometrical factor β^{α}. Finally, the Hamiltonian of the transmission line is

$$\hat{H}_{\text{line}} = \frac{1}{2}\int dx\, \{ \mathcal{C}[\hat{V}(x)]^2 + \mathcal{L}[\hat{I}(x)]^2 \}, \quad (2)$$

where $\hat{I}(x)$ and $\hat{V}(x)$ are electric current- and voltage-fields along the transmission line, with $\mathcal{C}$ and $\mathcal{L}$ the capacitance and inductance per unit length. The fields $\hat{I}(x)$ and $\hat{V}(x)$ are obtained through a standard canonical quantization procedure of the transmission line equations [33]; see Appendix A.

To allow for optimizing the performance of the device (see below), we assume the modes ω_k of the transmission line to be off-resonant with respect to the transition frequencies $\omega_{i,j}^{\alpha} = (\epsilon_i^{\alpha} - \epsilon_j^{\alpha})/\hbar$ of the transmons. The ensuing weak coupling allows for a perturbative treatment of the qubit-mode interaction. We make use of a unitary transformation of (1), $\hat{H} \to \mathcal{\hat{H}} = \hat{U}\hat{H}\hat{U}^{\dagger}$, in order to eliminate the transmission-line modes to lowest order. We choose the ansatz $\hat{U} = \exp[\hat{S} - \hat{S}^{\dagger}]$ and $\hat{S} = \sum_{\alpha,i} q_{i+1,i}^{\alpha} |i+1\rangle_{\alpha}{}_{\alpha}\langle i| \hat{Q}_i^{\alpha}$, where $\hat{Q}_i^{\alpha}$ is a linear form of the bosonic operators; see Appendix B for details. A rotating-wave approximation then provides us with an effective interaction between the qubits mediated via virtual-photon exchange [34],

$$\hat{H}_{\text{int}} = \sum_{ij} J_{ij} |i+1\rangle_{\text{L}}{}_{\text{L}}\langle i| \otimes |j\rangle_{\text{R}}{}_{\text{R}}\langle j+1| + \text{H.c.} \quad (3)$$

The effective couplings J_{ij} involve the commutator $[\hat{Q}_i^{\alpha}, [\hat{V}^{\beta}]^{\dagger}]$ between photonic field operators at the opposite ends of the transmission line that contributes the factor (with $\alpha = $ R, L and $\alpha \neq \beta$; we assume a long transmission line $\ell \gg \lambda$, where λ is the wavelength of the transmission line modes)

$$[\hat{Q}_i^{\alpha}, [\hat{V}^{\beta}]^{\dagger}] = \frac{1}{2\mathcal{C}\ell} \int d\omega \frac{\omega_{i+1,i}^{\alpha}}{(\omega_{i+1,i}^{\alpha} - \omega)^2}, \quad (4)$$

and its combination with the charge factors $q_{i+1,i}^{\alpha}$ provides us with the expression for the effective couplings,

$$J_{ij} = \frac{q_{i+1,i}^{\text{L}} q_{j,j+1}^{\text{R}}}{2\mathcal{C}\ell} \int d\omega \left[\frac{\omega_{i+1,i}^{\text{L}}}{(\omega_{i+1,i}^{\text{L}} - \omega)^2} + \frac{\omega_{j+1,j}^{\text{R}}}{(\omega_{j+1,j}^{\text{R}} - \omega)^2} \right].$$
$$(5)$$

Its inverse-length dependence $J_{ij} \propto 1/\ell$ is derived from the finite propagation velocity $v = 1/\sqrt{\mathcal{L}\mathcal{C}}$ of the electromagnetic modes inside the transmission line, implying an exchange time $\tau = \ell/v$ for the virtual photons that scales linearly with distance ℓ, thus reducing the coupling strength between the qubits as they are further separated. In the following, we assume that the transmission line modes are filtered to a frequency interval $[\omega_0 - \Delta\omega/2, \omega_0 + \Delta\omega/2]$, with $|\omega_0 - \omega_{i,j}^{\alpha}| \sim \omega_0$ and $\Delta\omega \ll \omega_0$, simplifying (5) to

$$J_{ij} = \frac{q_{i+1,i}^{\text{L}} q_{j,j+1}^{\text{R}}}{2\mathcal{C}\ell} \left[\frac{\Delta\omega\, \omega_{i+1,i}^{\text{L}}}{(\omega_{i+1,i}^{\text{L}} - \omega_0)^2} + \frac{\Delta\omega\, \omega_{j+1,j}^{\text{R}}}{(\omega_{j+1,j}^{\text{R}} - \omega_0)^2} \right]. \quad (6)$$

Furthermore, the transition energies of the target and demon qubits are chosen equal, $\omega_{1,0}^{\text{L}} = \omega_{1,0}^{\text{R}} = \omega_{1,0}$; otherwise, the interaction Hamiltonian H_{int} would not conserve energy, implying that the transition amplitudes $|i+1, j\rangle \to |i, j+1\rangle$ are suppressed due to oscillating phase factors (this feature can be used to switch the coupling on/off). With all other transitions chosen off-resonance, we can restrict the Hilbert space of the two-qubit system to the two lowest pairs of energy

states and arrive at the effective system Hamiltonian

$$\hat{H}_{qb} = \sum_{\alpha=L,R} \hbar\omega_{1,0}|1\rangle_{\alpha\,\alpha}\langle1| + J[|1,0\rangle\langle0,1| + |0,1\rangle\langle1,0|],$$

$$(7)$$

with a real-valued coupling constant $J \equiv J_{00}$,

$$J = \kappa^L \kappa^R \frac{\Delta\omega\,\omega_{1,0}}{(\omega_{1,0}-\omega_0)^2}\frac{h\upsilon}{\ell}.$$

$$(8)$$

The dimensionless qubit–transmission-line couplings κ^L and κ^R read (we use $q_{j,j+1}^\alpha = -2ie\beta^\alpha[(1+j)/2]^{1/2}(E_J^\alpha/8E_C^\alpha)^{1/4}$)

$$\kappa^\alpha = \beta^\alpha \left(\frac{E_J^\alpha}{2E_C^\alpha}\right)^{1/4}\sqrt{\frac{Z_0}{R_Q}},$$

$$(9)$$

with E_J^α and E_C^α the Josephson and charge energies of the transmon qubit α, $R_Q = h/e^2$ is the resistance quantum, and $Z_0 = 1/\upsilon\mathcal{C}$ is the characteristic impedance of the transmission line. For typical values $\beta \sim 0.1$, $Z_0 = 50\,\Omega$, and $E_J/E_C \sim 100$, one arrives at $\kappa \sim 0.01$.

III. DEMON (i)SWAP OPERATION

The XY-type interaction $H_{XY} = (J/2)[\hat{\sigma}_x\hat{\sigma}_x + \hat{\sigma}_y\hat{\sigma}_y]$ in the two-qubit Hamiltonian (7) naturally leads to an iSWAP quantum gate [35] when running the evolution (we define $\omega_J = J/\hbar$),

$$\hat{U}(\tau) = \begin{pmatrix} 1 & 0 & 0 & 0 \\ 0 & \cos(\omega_J\tau) & -i\sin(\omega_J\tau) & 0 \\ 0 & -i\sin(\omega_J\tau) & \cos(\omega_J\tau) & 0 \\ 0 & 0 & 0 & 1 \end{pmatrix}$$

$$(10)$$

during the time $\tau_{iSWAP} = \pi/2\omega_J$. On the other hand, the optimal interaction for the SWAP gate SWAP$(|\psi\rangle_L|\chi\rangle_R) = |\chi\rangle_L|\psi\rangle_R$ is the isotropic Heisenberg interaction $\hat{H}_{XYZ} = (J/2)[\hat{\sigma}_x\hat{\sigma}_x + \hat{\sigma}_y\hat{\sigma}_y + \hat{\sigma}_z\hat{\sigma}_z]$; acting during the time interval $\tau = h/4J$, it produces the unitary

$$\hat{U}_{SWAP} = e^{\frac{i\pi}{4}}\exp[-i(\pi/4)(\hat{\sigma}_x\hat{\sigma}_x + \hat{\sigma}_y\hat{\sigma}_y + \hat{\sigma}_z\hat{\sigma}_z)].\quad(11)$$

Given our setup, we have only the XY interaction at our disposal, from which one can generate a SWAP gate through a gate sequence involving square roots of iSWAP operations and single-qubit rotations, see Fig. 2,

$$\hat{U}_{SWAP} = e^{\frac{i\pi}{4}}\left[\hat{U}_y^\dagger\otimes\hat{U}_y^\dagger e^{-i\frac{\pi}{8}[\hat{\sigma}_x\hat{\sigma}_x + \hat{\sigma}_y\hat{\sigma}_y]}\hat{U}_y\otimes\hat{U}_y\right]$$
$$\times\left[\hat{U}_x^\dagger\otimes\hat{U}_x^\dagger e^{-i\frac{\pi}{8}[\hat{\sigma}_x\hat{\sigma}_x + \hat{\sigma}_y\hat{\sigma}_y]}\hat{U}_x\otimes\hat{U}_x\right]e^{-i\frac{\pi}{8}[\hat{\sigma}_x\hat{\sigma}_x + \hat{\sigma}_y\hat{\sigma}_y]},$$
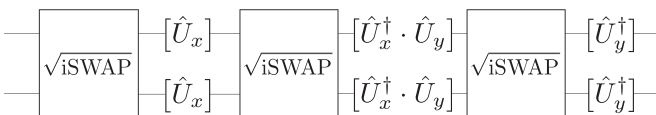
$$(12)$$

FIG. 2. Construction of the SWAP gate from three $\sqrt{\text{iSWAP}}$ gates augmented with single-qubit rotations $\hat{U}_x(\pi/2)$ and $\hat{U}_y(\pi/2)$ and its conjugates.
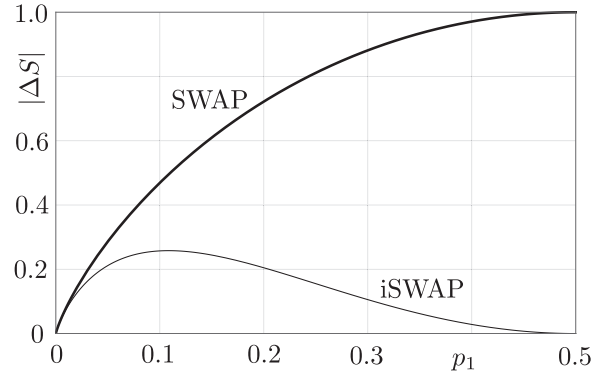

FIG. 3. Comparison of ideal entropy gain $\Delta S \leqslant 0$ of a thermal-state target qubit for the SWAP (thick line) and iSWAP (thin line) operation with a pure demon qubit as a function of the excited level occupation p_1. As $p_1 \to 0$, the target is already pure and the entropy gain vanishes.

where $\hat{U}_x = e^{-i\pi\hat{\sigma}_x/4}$ and $\hat{U}_y = e^{-i\pi\hat{\sigma}_y/4}$ are $\pi/2$ rotations around the x- and y-axis, respectively. Indeed, making use of the commutativity $[\hat{\sigma}_\alpha\otimes\hat{\sigma}_\alpha, \hat{\sigma}_\beta\otimes\hat{\sigma}_\beta] = 0$ for $\alpha, \beta = \{x, y, z\}$ and the unitary transformations of the Pauli matrices, $\hat{U}_x^\dagger\hat{\sigma}_y\hat{U}_x = -\hat{\sigma}_z$ and $\hat{U}_y^\dagger\hat{\sigma}_x\hat{U}_y = \hat{\sigma}_z$, one easily verifies the validity of Eq. (11). This SWAP gate implementation is twice as fast as the one with three iSWAP gates suggested in Ref. [35] and takes a time $\tau = 1.5\,\tau_{iSWAP}$ (we assume that all single-qubit rotations can be done infinitely fast); according to the discussion in Refs. [36,37], it is optimal.

The SWAP gate can fully purify any state $\hat{\rho}_t$ of the left (target) qubit by exchanging its state with a pure state $\hat{\rho}_d = |\chi\rangle\langle\chi|$ of the right (demon) qubit. Moreover, preparing the demon state with equal energy as the target qubit, $\text{Tr}\{\hat{H}^R\hat{\rho}_d\} = \text{Tr}\{\hat{H}^L\hat{\rho}_t\}$, one arrives at a device that nonlocally pushes the entropy of the target qubit to zero without changing its energy, thus defining our desired quantum Maxwell demon.

However, in practice the qubits are not ideal and prone to decoherence, thus restricting the available time required for the QMD operation. A way to relax this time restriction is to replace the SWAP gate by the naturally appearing iSWAP operation: since a full SWAP involves three $\sqrt{\text{iSWAP}}$ operations, an iSWAP demon performs its task at least 1.5 times faster, which is quite beneficial given the time constraints due to decoherence. Furthermore, as shown below, the iSWAP demon is less affected by decoherence. On the other hand, one has to admit that the iSWAP demon comes with a reduced purification power [38]; see Fig. 3: starting out with a thermal state of the target qubit $\hat{\rho}_{th} = p_0|0\rangle\langle0| + p_1|1\rangle\langle1|$ and an equal-energy pure state $\hat{\rho}_p = |\chi_{th}\rangle\langle\chi_{th}|$ with $|\chi_{th}\rangle = \sqrt{p_0}|0\rangle + \sqrt{p_1}|1\rangle$ for the demon qubit, the iSWAP-QMD generates a nonentangled but classically correlated state of the two qubits,

$$\hat{U}(\tau_{iSWAP})(\hat{\rho}_{th}\otimes\hat{\rho}_p) \stackrel{\tau_{iSWAP}}{\rightarrow} p_0[|\psi_-\rangle\langle\psi_-|]\otimes|0\rangle\langle0|$$
$$+ p_1[|\psi_+\rangle\langle\psi_+|\otimes|1\rangle\langle1|],\quad(13)$$

where $|\psi_\pm\rangle = \sqrt{p_0}|0\rangle \pm i\sqrt{p_1}|1\rangle$. The resulting entropy of the final target state $\hat{\rho}(\tau_{iSWAP}) = p_0|\psi_-\rangle\langle\psi_-| + p_1|\psi_+\rangle\langle\psi_+|$ is always bounded by the entropy of its original state; with
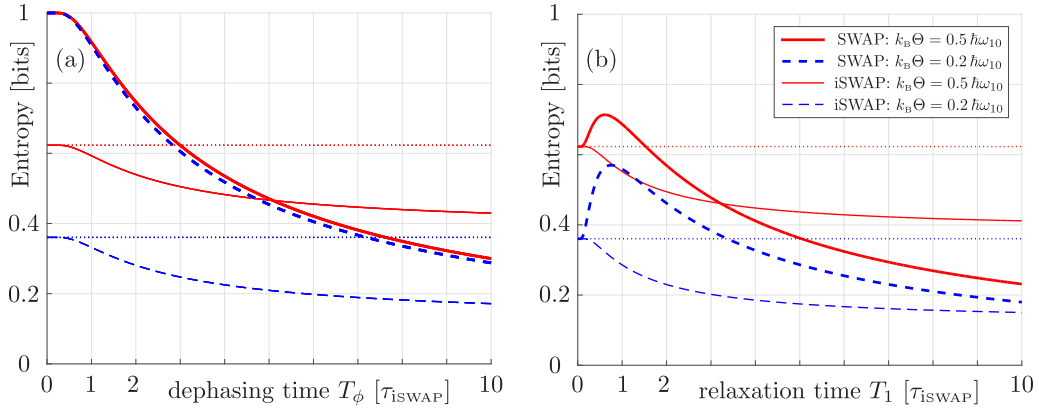
FIG. 4. (a) Final entropy of the target qubit (vertical axis in bits) after the execution of the SWAP-QMD (thick lines) and the iSWAP-QMD (thin lines) as a function of pure dephasing time T_ϕ (horizontal axis in units of $\tau_{\text{iSWAP}} = h/4J$, relaxation effects are neglected). The color/dashes indicate different temperatures of the qubit environment, and the dotted lines mark the level of the target qubit's initial entropy. (b) Final entropy of the target qubit as a function of relaxation time T_1 in the absence of dephasing effects.

$S[\hat{\rho}]$ the von Neumann entropy of the state $\hat{\rho}$, the iSWAP QMD provides an entropy reduction $\Delta S = S[\hat{\rho}(\tau_{\text{iSWAP}})] - S[\hat{\rho}_{\text{th}}] \leqslant 0$ with the equal sign realized for the chaotic state with $p_0 = p_1 = 1/2$. Note that, during the operation of the iSWAP gate, the average energy $p_1 \hbar \omega_{1,0}$ of the target qubit remains constant.

As announced above, dephasing and relaxation affect the iSWAP- and SWAP-QMDs quite differently, with the iSWAP-QMD performing better at short dephasing/relaxation times, while the SWAP-QMD ultimately outperforms the iSWAP-QMD at long dephasing/relaxation times due to its higher purification power. Including dephasing and relaxation in the demon's evolution, we have to replace the unitary $\hat{U}(\tau)$ in (10) by a channel $\Phi(\tau)$ that accounts for the environment; see Appendix C. We assume our qubits interact with their local environments, each in thermal equilibrium at some temperature Θ, and we adopt the above initial states $\hat{\rho}_{\text{th}}$ and $\hat{\rho}_{\text{p}}$ for the target and demon qubits with $p_1/p_0 = \exp(-\hbar \omega_{1,0}/k_{\text{B}}\Theta)$. Solving the corresponding Lindblad master equations [39] numerically, we determine the time evolution of the entropies for both demons and for the two cases of pure dephasing and relaxation. In Fig. 4, we show the target qubit's final entropy for different ratios $T_\phi/\tau_{\text{iSWAP}}$ [pure dephasing, in (a)] and T_1/τ_{iSWAP} [relaxation, in (b)] and for different temperatures.

As expected, short dephasing and relaxation times destroy the purification power of both demons. Increasing the dephasing and relaxation times in Fig. 4, we find that the iSWAP-QMD performs better at small T_1 and T_ϕ, while good qubits with large T_1 and T_ϕ profit from the better purification power of the SWAP operation. An additional surprise is that the SWAP-QMD fails completely at small T_1 and T_ϕ where the final entropy turns out to be higher [and even maximal for $T_\phi/\tau_{\text{iSWAP}} \to 0$ in Fig. 4(a)] than the initial one. We attribute this entropy increase to the action of the intermediate single-qubit rotations in the SWAP operation and its extreme sensitivity to decoherence.

Indeed, consider the extreme case of strong dephasing with T_ϕ much shorter than the duration of the iSWAP gate, $T_\phi \ll \tau_{\text{iSWAP}}$, but longer than or compatible with the duration of one-qubit operations. Given such a strong dephasing leads to a rapid collapse of the qubits to a product of thermal states,

$\hat{\rho}_{\text{th}} \otimes \hat{\rho}_{\text{p}} \overset{\sqrt{\text{iSWAP}}}{\to} \hat{\rho}_{\text{th}} \otimes \hat{\rho}_{\text{th}}$, implying that the entropy of the target qubit is not changed; see Fig. 4. Going on with the SWAP demon, the subsequent $\pi/2$ rotations $\hat{U}_x$ take the (now thermal) qubits out of the decoherence-free subspace, $\hat{\rho}_{\text{th}} \to \hat{\rho}_{\text{rot}} = \hat{U}_x \hat{\rho}_{\text{th}} \hat{U}_x^\dagger \equiv (1/2)\mathbb{1} + \hat{\sigma}_y(p_0 - p_1)/2$, and the subsequent evolution brings both qubits into the maximally mixed state, $\hat{\rho}_{\text{rot}} \otimes \hat{\rho}_{\text{rot}} \overset{\sqrt{\text{iSWAP}}}{\to} (1/2)\mathbb{1} \otimes (1/2)\mathbb{1}$.

The same argument is valid for strong relaxation $T_1 \to 0$: the evolution rapidly takes the pair of qubits into a product of thermal states, while subsequent $\hat{U}_x$ rotations take them out of the equilibrium with their local environment, $\hat{\rho}_{\text{th}} \to \hat{\rho}_{\text{rot}}$. During the next $\sqrt{\text{iSWAP}}$ gate, both qubits relax back to the thermal equilibrium state, $\hat{\rho}_{\text{rot}} \otimes \hat{\rho}_{\text{rot}} \overset{\sqrt{\text{iSWAP}}}{\to} \hat{\rho}_{\text{th}} \otimes \hat{\rho}_{\text{th}}$, keeping the target qubit in the original entropy state. However, for a moderately strong relaxation strength, the state $\hat{\rho}_{\text{rot}}$ may not have enough time to relax back into the thermal state $\hat{\rho}_{\text{th}}$ during the square-root iSWAP time $\tau_{\text{iSWAP}}/2$ and thus ends up in a higher entropy state. This explains the nonmonotonic behavior of the entropy of the target qubit at short relaxation times in Fig. 4(b). The above discussion lets us conclude that the iSWAP-QMD is less sensitive to dephasing and relaxation than its SWAP analog; only for long dephasing and relaxation times $T_\phi, T_1 \gg \tau_{\text{iSWAP}}$ does the better purification power of the SWAP gate beat the performance of the iSWAP-demon.

IV. OPERATIONAL REQUIREMENTS FOR THE DEMON

The functionality of the iSWAP demon depends critically on its environment, of which the transmission line is an integral part. A large separation between the target and demon qubits reduces the coupling J and thus enhances the operation time τ_{iSWAP}, which is in conflict with the finite decoherence time T_2; as a result, we obtain a limit ℓ of the demon's extension; see Sec. IV A. Second, the presence of the transmission line will itself increase both the dephasing and the relaxation rate of the qubits. While dephasing due to the thermally excited bosonic modes will limit the operational temperature of the transmission line (see Sec. IV B 1), we find that the enhanced qubit relaxation due to a lossy transmission line

(Purcell effect, see Sec. IV B 2) is not (yet) relevant in our setup.

A. Demon extension

Given a decoherence time $T_2 = (1/2T_1 + 1/T_\phi)^{-1}$, we estimate the possible extension ℓ of the demon. To successfully realize an iSWAP operation, the condition $\tau_{\text{iSWAP}} \sim T_2$ has to be satisfied. Choosing the specific arrangement $\omega_{1,0} = 2\omega_0$ for the resonator and qubit transition frequencies and similar target and demon qubits with $\kappa^L = \kappa^R = \kappa$, one finds that

$$T_2 \sim \frac{\ell}{v} \frac{1}{8\kappa^2} \frac{\omega_0}{\Delta\omega}. \quad (14)$$

Assuming typical values $v \sim 2c/3$, $\omega_0 \sim 2\pi \times 5$ GHz, and $\Delta\omega \sim 2\pi \times 500$ MHz, we find that typical coherence times $T_2 \sim 50$–$250\ \mu$s allow for an extension of the demon over macroscopic lengths $\ell \sim 1.0$–5.0 m.

B. Dephasing and relaxation due to the transmission line

1. Dephasing and transmission line temperature

So far, we have assumed that the transmission line is kept at low temperature such that electromagnetic modes within its bandwidth $[\omega_0 - \Delta\omega/2, \omega_0 + \Delta\omega/2]$ are not thermally excited. Given the possibility for a macroscopic separation ℓ, a question of much technological interest then is whether the QMD can be operated through a hot and thus less quantum environment. Indeed, at finite temperatures a thermal voltage noise appears in the transmission line that causes dephasing of the qubits. The dephasing due to the presence of a (hot) transmission line is described via the dispersive shift of the qubit energy levels induced by the fluctuating voltages at the ends of the transmission line. The corresponding qubit-dephasing Hamiltonian is given by $\hat{H}_{\text{sh}} = \sum_{\alpha=L,R} [|0\rangle_{\alpha\ \alpha}\langle 0| - |1\rangle_{\alpha\ \alpha}\langle 1|] \otimes \hat{B}^\alpha(x^\alpha)$, where the operators $\hat{B}^\alpha(x^\alpha) = \sum_{n,m} b_{nm}(x^\alpha) \hat{a}_n^\dagger \hat{a}_m$ describe the coupling to the transmission line modes of the electromagnetic environment; see Appendix B (here, $\hat{a}_n$ denote bosonic operators of the transmission line). The presence of thermal modes in the transmission line then modifies the level separation of the qubit and induces dephasing at a rate (see Appendix D 1)

$$\gamma_\phi^{\alpha\alpha'} = 32\pi \, (\kappa^\alpha \kappa^{\alpha'})^2 N_{\omega_0}(1 + N_{\omega_0}) \, \Delta\omega$$
$$\times \left[\frac{\omega_{\text{an}}^\alpha \omega_0}{(\omega_{1,0}^\alpha - \omega_0)(\omega_{2,1}^\alpha - \omega_0)} \right]$$
$$\times \left[\frac{\omega_{\text{an}}^{\alpha'} \omega_0}{(\omega_{1,0}^{\alpha'} - \omega_0)(\omega_{2,1}^{\alpha'} - \omega_0)} \right], \quad (15)$$

where N_ω is the Bose-Einstein distribution function and $\omega_{\text{an}}^\alpha = \omega_{1,0}^\alpha - \omega_{2,1}^\alpha$ are the anharmonicities of the transmon spectra. Remarkably, the dephasing rate scales as $\gamma_\phi \propto \kappa^4$, while the coupling constant $J \propto \kappa^2$; see Eq. (8); both of them are linear in the frequency bandwidth $\Delta\omega$. Therefore, installing a small coupling κ, one can keep the qubit dephasing rates small while leaving a sufficiently strong coupling between the qubits. The iSWAP-QMD device is functional when $\gamma_\phi \tau_{\text{iSWAP}} \leqslant 1$, which

translates into a requirement on the photon occupation number

$$N_{\omega_0}(1 + N_{\omega_0}) \leqslant \left[8\pi\kappa^2 \frac{\omega_0 \ell}{v} \frac{\omega_0}{\omega_{1,0}} \left(\frac{\omega_{\text{an}}}{\omega_{2,1} - \omega_0} \right)^2 \right]^{-1}. \quad (16)$$

For $\omega_0 \sim 2\pi \times 5$ GHz, $v \sim 2c/3$, and $\omega_{\text{an}} \sim 2\pi \times 300$ MHz, we find that $N_{\omega_0}(1 + N_{\omega_0}) \leqslant 1000$ m/ℓ, which translates to a corresponding temperature range $7.5 \geqslant \Theta_{\text{line}} \geqslant 3.5$ K for $1 \leqslant \ell \leqslant 5.0$ m. Hence, the transmission line can reside at a temperature that is about two orders of magnitude higher than the typical operation temperature $\Theta_{\text{qubit}} \sim 20$ mK of the superconducting qubits.

2. Relaxation through the Purcell effect

Finally, we study the consequences of losses in the transmission line. Indeed, a finite loss rate γ_{line} in the transmission line induces an enhanced decay of the qubit excited state via the Purcell effect (see Appendix D 2),

$$\gamma_{\text{Pur}}^\alpha = 2 \, \gamma_{\text{line}} \, (\kappa^\alpha)^2 \frac{\Delta\omega \, \omega_0}{(\omega_{1,0}^\alpha - \omega_0)^2}. \quad (17)$$

For commercially available coaxial cables with an attenuation constant ~ 0.1 dB/m one has $\gamma_{\text{line}} \sim 4.6$ MHz, and choosing parameters as above results in a lifetime $\gamma_{\text{Pur}}^{-1} \sim 9$ ms that is long compared to the relaxation time T_1 assumed above. Hence, we conclude that the presence of the transmission line does not significantly reduce the performance of the qubit's characteristics that we have assumed above.

V. CONCLUSION

In conclusion, we have proposed a realistic design for a spatially distributed quantum Maxwell demon based on a cQED platform. The transmon-type target and demon qubits are capacitively coupled via the electromagnetic modes of a transmission line; its nonresonant coupling allows us to keep the line at high temperatures, of order Kelvin, while the resonant coupling of other designs [16] requires a cold line. The device serves to reduce the entropy of the target qubit via exchange of its state with a higher-purity demon state. Previous demons, both local [18] and extended [10], were based on SWAP or partial-SWAP operations involving multiple CNOT gates; here, we have proposed to reduce the demon's complexity via operating on the "machine code" level by directly exploiting the XY-type coupling between the qubits. The resulting iSWAP gate then provides limited purification power to the demon but behaves more benevolently with respect to decoherence. Our estimates show that the target qubit can be purified "from a distance," with the demon qubit located a macroscopic distance of order meters away. The proposed setup can be implemented with present-day technology.

APPENDIX A: TRANSMISSION LINE

An ideal lossless transmission line can be modeled as a pair of uniform conductors separated by a dielectric medium; it is characterized by a series of inductances $\mathcal{L}$ (in Henry/m) and shunt capacitances $\mathcal{C}$ (Farad/m) [32]. The voltage $V(x, t)$ and current $I(x, t)$ along the transmission line are described by the transmission line equations

$$\partial_x V = -\mathcal{L}\, \partial_t I, \quad \partial_x I = -\mathcal{C}\, \partial_t V. \quad \text{(A1)}$$

Introducing the potential $\varphi(x, t)$ and expressing the voltage and current via $V(x, t) = \sqrt{\mathcal{L}}\, \partial_t \varphi(x, t)$ and $I(x, t) = -\partial_x \varphi(x, t)/\sqrt{\mathcal{L}}$, the transmission line equations reduce to a standard wave equation (with $\dot{\varphi} = \partial_t \varphi$ and $\varphi' = \partial_x \varphi$),

$$\ddot{\varphi} - c^2 \varphi'' = 0, \quad \text{(A2)}$$

where $c = 1/\sqrt{\mathcal{L}\mathcal{C}}$ is the wave velocity.

The quantization of the transmission line fields [33] is done via standard canonical quantization. The classical equation of motion (A2) derives from minimizing the classical action $S = \int dt\, dx\, L(\dot{\varphi}, \varphi)$ with the Lagrangian density

$$L(\dot{\varphi}, \varphi) = \frac{1}{2}[(\dot{\varphi}/c)^2 - (\varphi')^2]. \quad \text{(A3)}$$

Introducing the conjugated field $\pi(x) = \partial L/\partial \dot{\varphi} = \dot{\varphi}/c^2$ provides us with the Hamiltonian $H(\pi, \varphi) = \int dx\, \pi(x) \dot{\varphi}(x) - L(\pi, \varphi)$,

$$H(\pi, \varphi) = \frac{1}{2} \int dx [c^2 \pi^2(x) + \varphi'^2(x)]. \quad \text{(A4)}$$

Going back to the original fields $V(x) = c^2 \sqrt{\mathcal{L}}\, \pi(x)$ and $I(x) = -\varphi'(x)/\sqrt{\mathcal{L}}$, we obtain the transmission line Hamiltonian

$$H = \frac{1}{2} \int dx [\mathcal{C} V^2(x) + \mathcal{L} I^2(x)]. \quad \text{(A5)}$$

The canonical quantization maps the classical fields to operators $\varphi(x) \to \hat{\varphi}(x)$ and $\pi(x) \to \hat{\pi}(x)$ with commutation relations $[\hat{\varphi}(x), \hat{\varphi}(y)] = [\hat{\pi}(x), \hat{\pi}(y)] = 0$ and $[\hat{\varphi}(x), \hat{\pi}(y)] = i\hbar \delta(x - y)$. Introducing the transmission line modes

$$\hat{\varphi}(x) = c \sum_k \left(\frac{\hbar}{2\omega_k \ell}\right)^{1/2} (\hat{a}_k e^{ikx} + \hat{a}_k^\dagger e^{-ikx}), \quad \text{(A6)}$$

$$\hat{\pi}(x) = -\frac{i}{c} \sum_k \left(\frac{\hbar \omega_k}{2\ell}\right)^{1/2} (\hat{a}_k e^{ikx} - \hat{a}_k^\dagger e^{-ikx}), \quad \text{(A7)}$$

we go over to bosonic annihilation and creation operators $\hat{a}_k$ and $\hat{a}_k^\dagger$ with commutators $[\hat{a}_k, \hat{a}_{k'}^\dagger] = \delta_{kk'}$, dispersion $\omega_k = c|k|$, and $\ell \to \infty$ is the length of the transmission line. The

Hamiltonian (A4) then transforms into the standard form

$$H(\pi, \varphi) \to \hat{H}_{\text{line}} = \frac{1}{2} \sum_k \hbar \omega_k (\hat{a}_k^\dagger \hat{a}_k + \hat{a}_k \hat{a}_k^\dagger). \quad \text{(A8)}$$

The voltage and current operators derive from the mode operators $\hat{a}_k$ and $\hat{a}_k^\dagger$ via

$$\hat{V}(x) = -i \sum_k \left(\frac{\hbar \omega_k}{2C_r}\right)^{1/2} (\hat{a}_k e^{ikx} - \hat{a}_k^\dagger e^{-ikx})$$

$$\equiv \sum_k \hat{V}_k e^{ikx} + \text{H.c.}, \quad \text{(A9)}$$

$$\hat{I}(x) = -i \sum_k \text{sgn}(k) \left(\frac{\hbar \omega_k}{2L_r}\right)^{1/2} (\hat{a}_k e^{ikx} - \hat{a}_k^\dagger e^{-ikx})$$

$$\equiv \sum_k \hat{I}_k e^{ikx} + \text{H.c.}, \quad \text{(A10)}$$

where $C_r = \mathcal{C}\ell$ and $L_r = \mathcal{L}\ell$ are the total capacitance and inductance of the transmission line. The k-components of the voltage and current operators are linearly related through a transmission line impedance $Z_0 = \sqrt{\mathcal{L}/\mathcal{C}}$,

$$\hat{V}_k = Z_0 \text{sgn}(k) \hat{I}_k. \quad \text{(A11)}$$

For an open transmission line, we have to impose the boundary conditions $\hat{I}(x = \pm\ell/2) = 0$, resulting in a discrete level spectrum with wave numbers $k_n = \pi n/\ell$, $n \geqslant 0$, describing even and odd modes

$$\hat{V}(x) = -i \sum_n \left(\frac{\hbar \omega_n}{C_r}\right)^{1/2} \varphi_n(x) \hat{a}_n + \text{H.c.}, \quad \text{(A12)}$$

where

$$\varphi_n(x) = \begin{cases} \cos(\pi n x/\ell), & n \text{ even,} \\ i \sin(\pi n x/\ell), & n \text{ odd.} \end{cases} \quad \text{(A13)}$$

APPENDIX B: INTERACTION HAMILTONIAN FOR TRANSMON QUBITS

We wish to eliminate the transmission line modes in the Hamiltonian (1) to lowest order in the bosonic operators a_n; this will provide us with the effective qubit-qubit coupling and higher-order terms including a dispersive shift describing transmission-line induced dephasing. We use a perturbative scheme that is valid in the off-resonant regime $|\omega_{1,0}^\alpha - \omega_0| \sim \omega_0$. We perform a unitary transformation, $\hat{H} \to \hat{\mathcal{H}} = \hat{U} \hat{H} \hat{U}^\dagger$ with $\hat{U} = \exp[\hat{S} - \hat{S}^\dagger]$, and we seek an operator $\hat{S} = \sum_{\alpha,i} q_{i+1,i}^\alpha |i+1\rangle_\alpha {}_\alpha\langle i| \hat{Q}_i^\alpha$ that eliminates the terms linear in a_n within the expansion $\hat{\mathcal{H}} \approx \hat{H} + [\hat{S}, \hat{H}] + [\hat{S}, \hat{H}]^\dagger + \cdots$. This is achieved by the choice

$$\hat{Q}_i^\alpha = -i \sum_n \left(\frac{\omega_n}{\hbar C_r}\right)^{1/2} \frac{\varphi_n(x_\alpha)}{\omega_{i+1,i}^\alpha - \omega_n} \hat{a}_n. \quad \text{(B1)}$$

The transformed Hamiltonian then takes the form

$$\hat{\mathcal{H}} \approx \hat{H}_{\text{transmon}} + \hat{H}_{\text{bath}} + \hat{H}_{\text{sh}} + \hat{H}_{\text{2ph}} + \hat{H}_{\text{int}}, \quad \text{(B2)}$$

where $\hat{H}_{\text{bath}} = \sum_n \hbar \omega_n \hat{a}_n^\dagger \hat{a}_n$ is the transmission line Hamiltonian and $\hat{H}_{\text{sh}}$ describes the dispersive shift of the transmon's energy levels due to the off-resonant interaction

with the transmission line modes,

$$\hat{H}_{\mathrm{sh}} = |q_{i+1,i}^{\alpha}|^2 \sum_{i,\alpha} |i+1\rangle_{\alpha \, \alpha}\langle i+1| \big(\hat{Q}_i^{\alpha}[\hat{V}^{\alpha}]^{\dagger} + \hat{V}^{\alpha}[\hat{Q}_i^{\alpha}]^{\dagger}\big)$$

$$- |q_{i+1,i}^{\alpha}|^2 \sum_{i,\alpha} |i\rangle_{\alpha \, \alpha}\langle i| \big([\hat{V}^{\alpha}]^{\dagger}\hat{Q}_i^{\alpha} + [\hat{Q}_i^{\alpha}]^{\dagger}\hat{V}^{\alpha}\big). \quad \text{(B3)}$$

The contribution $\hat{H}_{2\mathrm{ph}}$ describes the next-order two-photon interaction process,

$$\hat{H}_{2\mathrm{ph}} = \sum_{\alpha,i} |i+2\rangle_{\alpha \, \alpha}\langle i| \otimes \hat{\eta}_i^{\alpha} + \text{H.c.}, \quad \text{(B4)}$$

where $\hat{\eta}_i^{\alpha} = q_{i+i,i}^{\alpha} q_{i+2,i+1}^{\alpha} (\hat{Q}_{i+1}^{\alpha} - \hat{Q}_i^{\alpha})\hat{V}^{\alpha}$. Finally, the term $\hat{H}_{\mathrm{int}}$ describes the directly induced interaction between the transmon qubits,

$$\hat{H}_{\mathrm{int}} = \sum_{\alpha \neq \beta} \sum_{i,j} |i+1\rangle_{\alpha \, \alpha}\langle i| \otimes |j\rangle_{\beta \, \beta}\langle j+1|$$

$$\times q_{i+1,i}^{\alpha} q_{j,j+1}^{\beta} \big[\hat{Q}_i^{\alpha}, [\hat{V}^{\beta}]^{\dagger}\big] + \text{H.c.} \quad \text{(B5)}$$

The effective coupling constant involves the commutator of the electromagnetic field operators at the opposite ends of the transmission line. Making use of the explicit form of the operators $\hat{V}^{\alpha}$ and $\hat{Q}_i^{\alpha}$, see Eqs. (A12) and (B1), one finds

$$\big[\hat{Q}_i^{\alpha}, [\hat{V}^{\beta}]^{\dagger}\big] = \sum_{n \text{ even}} \frac{\omega_n}{C_r} \frac{\cos(\pi n x^{\alpha}/\ell)\cos(\pi n x^{\beta}/\ell)}{\omega_{i+1,i}^{\alpha} - \omega_n}$$

$$+ \sum_{n \text{ odd}} \frac{\omega_n}{C_r} \frac{\sin(\pi n x^{\alpha}/\ell)\sin(\pi n x^{\beta}/\ell)}{\omega_{i+1,i}^{\alpha} - \omega_n}. \quad \text{(B6)}$$

In particular, for transmon qubits located at the opposite ends $x^{\alpha} = -x^{\beta} = \ell/2$ of the transmission line, one has

$$\big[\hat{Q}_i^{\alpha}, [\hat{V}^{\beta}]^{\dagger}\big] = \frac{1}{C_r} \sum_{k=1}^{\infty} \frac{(\omega_{2k} - \omega_{2k-1})\,\omega_{i+1,i}^{\alpha}}{(\omega_{i+1,i}^{\alpha} - \omega_{2k})(\omega_{i+1,i}^{\alpha} - \omega_{2k-1})}. \quad \text{(B7)}$$

Going to the continuous limit $\sum_k \to \int \frac{\ell d\omega}{2\pi c}$ one finds

$$\big[\hat{Q}_i^{\alpha}, [\hat{V}^{\beta}]^{\dagger}\big] = \frac{1}{2C_r} \int d\omega \frac{\omega_{i+1,i}^{\alpha}}{(\omega_{i+1,i}^{\alpha} - \omega)^2}. \quad \text{(B8)}$$

Substituting this expression into Eq. (B5), one finally arrives at the qubit-qubit coupling constants J_{ij} given in Eq. (5) of the main text.

APPENDIX C: PHENOMENOLOGICAL LINDBLAD ANALYSIS

1. Qubit relaxation

We assume that each qubit interacts with its local environment, and we describe the evolution of the two-qubit density matrix $\hat{\rho}(t)$ by the Lindblad equation,

$$\frac{d\hat{\rho}(t)}{dt} = -i[\hat{H}(t), \hat{\rho}(t)] + \sum_{\alpha=\mathrm{L,R}} \mathcal{D}_{\mathrm{rel}}^{\alpha}[\hat{\rho}(t)], \quad \text{(C1)}$$

where $\hat{H}(t)$ is the time-dependent Hamiltonian, which describes the sequence of one- and two-qubit operations applied

during the execution of the SWAP and iSWAP Maxwell demon, and $\mathcal{D}_{\mathrm{rel}}^{\alpha}[\hat{\rho}]$ is the dissipator that describes the excitation/relaxation processes for the qubits $\alpha = \mathrm{L}, \mathrm{R}$,

$$\mathcal{D}_{\mathrm{rel}}^{\alpha}[\hat{\rho}] = \sum_{\mu=\pm} \gamma_{\mu}^{\alpha} \Big(\hat{\sigma}_{\mu}^{\alpha} \hat{\rho} \, [\hat{\sigma}_{\mu}^{\alpha}]^{\dagger} - \frac{1}{2}\{[\hat{\sigma}_{\mu}^{\alpha}]^{\dagger}\hat{\sigma}_{\mu}^{\alpha}, \hat{\rho}\}\Big). \quad \text{(C2)}$$

Here, $\hat{\sigma}_-^{\alpha} = |0\rangle_{\alpha \, \alpha}\langle 1|$ and $\hat{\sigma}_+^{\alpha} = |1\rangle_{\alpha \, \alpha}\langle 0|$ describe the relaxation and excitation processes with rates $\gamma_{\pm}^{\alpha} > 0$, and $\{\cdot, \cdot\}$ is the anticommutator. If both local environments are in thermal equilibrium at a temperature Θ, then $\gamma_+^{\alpha} = \gamma_-^{\alpha} \exp(-\beta\hbar\omega_{1,0})$ with $\beta = 1/k_B\Theta$.

We assume that the target qubit on the left initially is in thermal equilibrium with its environment, $\hat{\rho}_t(0) = \hat{\rho}_{\mathrm{th}} = p_0|0\rangle_{\mathrm{L \, L}}\langle 0| + p_1|1\rangle_{\mathrm{L \, L}}\langle 1|$, where $p_0 = [1 + \exp(-\beta\hbar\omega_{1,0})]^{-1}$ and $p_1 = [1 + \exp(\beta\hbar\omega_{1,0})]^{-1}$ are equilibrium occupation probabilities. In contrast, the demon qubit on the right is prepared in the equal-energy pure state, $\hat{\rho}_d(0) = \hat{\rho}_p = |\chi_0\rangle\langle\chi_0|$ with $|\chi_0\rangle = \sqrt{p_0}|0\rangle_{\mathrm{R}} + \sqrt{p_1}|1\rangle_{\mathrm{R}}$.

The execution of the iSWAP operation in the presence of the relaxation processes is described by Eq. (C1) with the constant Hamiltonian,

$$\hat{H}(t) = J\begin{bmatrix} 1 & 0 & 0 & 0 \\ 0 & 0 & 1 & 0 \\ 0 & 1 & 0 & 0 \\ 0 & 0 & 0 & 1 \end{bmatrix} \quad \text{(C3)}$$

acting during the time interval $0 < t \leqslant \tau_{\mathrm{iSWAP}} = h/4J$. The Lindblad equation (C1) with the Hamiltonian (C3) describes the linear evolution of the 16 components of the density matrix $\hat{\rho}(t)$, and its formal result can be written in the form of a quantum channel,

$$\hat{\rho}(t = \tau_{\mathrm{iSWAP}}) = \Phi_{\mathrm{iSWAP}}[\hat{\rho}_t(0) \otimes \hat{\rho}_d(0)]. \quad \text{(C4)}$$

For its numerical solution, we assume that $\gamma_{\pm,\mathrm{L}} = \gamma_{\pm,\mathrm{R}} = \gamma_{\pm}$, such that the result merely depends on the two dimensionless parameters γ_-/J and $\beta\hbar\omega_{1,0}$.

On the other hand, the SWAP demon involves the consecutive transformations of the density matrix $\hat{\rho}$ according to the quantum circuit shown in Fig. 2 of the main text,

$$\hat{\rho}(0) \to \hat{\rho}_1' = \Phi_{\sqrt{\mathrm{iSWAP}}}[\hat{\rho}(0)]$$

$$\to \hat{\rho}_1 = [\hat{U}_x \otimes \hat{U}_x] \cdot \hat{\rho}_1' \cdot [\hat{U}_x^{\dagger} \otimes \hat{U}_x^{\dagger}]$$

$$\to \hat{\rho}_2' = \Phi_{\sqrt{\mathrm{iSWAP}}}[\hat{\rho}_1]$$

$$\to \hat{\rho}_2 = [\hat{U}_y\hat{U}_x^{\dagger} \otimes \hat{U}_y\hat{U}_x^{\dagger}] \cdot \hat{\rho}_2' \cdot [\hat{U}_x\hat{U}_y^{\dagger} \otimes \hat{U}_x\hat{U}_y^{\dagger}]$$

$$\to \hat{\rho}_3' = \Phi_{\sqrt{\mathrm{iSWAP}}}[\hat{\rho}_2]$$

$$\to \hat{\rho}_3 = [\hat{U}_y^{\dagger} \otimes \hat{U}_y^{\dagger}] \cdot \hat{\rho}_3' \cdot [\hat{U}_y \otimes \hat{U}_y], \quad \text{(C5)}$$

where $\hat{U}_x = \exp[-i\pi\,\hat{\sigma}_x/4]$ is a spin-1/2 rotation by $\pi/2$ around the x-axis, and $\Phi_{\sqrt{\mathrm{iSWAP}}}$ is a quantum channel, corresponding to $\sqrt{\mathrm{iSWAP}}$ execution in the presence of decoherence. In the above transformation, we have assumed that the one-qubit rotations take a negligible time in comparison with the $\sqrt{\mathrm{iSWAP}}$ operation, and therefore the relaxation processes can be neglected during their execution. In Fig. 4(b), we show the von Neumann entropy $S[\hat{\rho}]$ evaluated for the SWAP and

iSWAP channels for a qubit evolution including relaxation processes characterized by $\gamma_- = 1/T_1$.

2. Qubit dephasing

Dephasing is phenomenologically accounted for by the dissipator

$$\mathcal{D}_{\text{dph}}[\hat{\rho}] = \sum_{\alpha,\alpha'} \gamma_\phi^{\alpha\alpha'} \left(\hat{\sigma}_z^\alpha \hat{\rho} \, \hat{\sigma}_z^{\alpha'} - \{ \hat{\sigma}_z^{\alpha'} \hat{\sigma}_z^\alpha, \hat{\rho} \}/2 \right), \quad \text{(C6)}$$

where $\hat{\sigma}_z^\alpha = |0\rangle_{\alpha\,\alpha}\langle 0| - |1\rangle_{\alpha\,\alpha}\langle 1|$ and $\gamma_\phi^{\alpha\alpha'}$ are pure dephasing rates. In our numerical evaluation of the channel $\Phi(t)$, we use the phenomenological parameter $\gamma_\phi^{\alpha\alpha'} = 1/T_\phi$. In Fig. 4(a), we show the von Neumann entropy $S[\hat{\rho}]$ evaluated for the SWAP and iSWAP channels for a qubit evolution with pure dephasing processes.

APPENDIX D: TRANSMISSION-LINE INDUCED DECOHERENCE

The transmission line induces qubit dephasing due to the presence of thermal photons, and we present a microscopic analysis of this effect in Appendix D 1. Furthermore, a lossy transmission line enhances the qubit's relaxation rate via the Purcell effect, which is studied in Appendix D 2.

1. Qubit dephasing

We determine the transmission-line induced dephasing rate of the qubit. The latter can be derived microscopically by accounting for the sensitivity of the qubit's energy levels to the presence of photons in the transmission line, as described by the dispersive shift $\hat{H}_{\text{sh}}$ in Eq. (B3). In the qubit subspace, this Hamiltonian can be written as

$$\hat{H}_{\text{sh}} = \sum_\alpha \hat{\sigma}_z^\alpha \otimes \hat{B}^\alpha(x^\alpha), \quad \text{(D1)}$$

with the bosonic fields $\hat{B}^\alpha(x^\alpha)$ given by

$$\hat{B}^\alpha(x^\alpha) = \frac{1}{2} \sum_{n,m} \left(\frac{\omega_n \omega_m}{C_r^2} \right)^{1/2} \left\{ \frac{|q_{2,1}^\alpha|^2}{\omega_{2,1}^\alpha - \omega_n} - \frac{2|q_{1,0}^\alpha|^2}{\omega_{1,0}^\alpha - \omega_n} \right.$$
$$\left. + \frac{|q_{2,1}^\alpha|^2}{\omega_{2,1}^\alpha - \omega_m} - \frac{2|q_{1,0}^\alpha|^2}{\omega_{1,0}^\alpha - \omega_m} \right\} \varphi_n^*(x^\alpha) \varphi_m(x^\alpha) \, \hat{a}_n^\dagger \hat{a}_m. \quad \text{(D2)}$$

The second qubit level $i = 2$ appears through the terms $i = 1$ in the second line of Eq. (B3). Using the relation $|q_{2,1}^\alpha|^2 = 2|q_{1,0}^\alpha|^2$, this expression simplifies to

$$\hat{B}^\alpha(x^\alpha) = (\kappa^\alpha)^2 \frac{hv}{\ell} \sum_{n,m} \left\{ \frac{\omega_{\text{an}}^\alpha \sqrt{\omega_n \omega_m}}{(\omega_{1,0}^\alpha - \omega_n)(\omega_{2,1}^\alpha - \omega_n)} \right.$$
$$\left. + \frac{\omega_{\text{an}}^\alpha \sqrt{\omega_n \omega_m}}{(\omega_{1,0}^\alpha - \omega_m)(\omega_{2,1}^\alpha - \omega_m)} \right\} \varphi_n^*(x^\alpha) \varphi_m(x^\alpha) \, \hat{a}_n^\dagger \hat{a}_m, \quad \text{(D3)}$$

where $\omega_{\text{an}}^\alpha = \omega_{1,0}^\alpha - \omega_{2,1}^\alpha$ is the anharmonicity of the transmon spectrum. The dispersive shift Eq. (D1) introduces fluctuating phases in the qubits, and their thermal averaging provides us

with the dephasing rates; these are given by the irreducible correlators of the bosonic fields [39],

$$\gamma_\phi^{\alpha\alpha'} = \frac{1}{\hbar^2} \int d\tau \langle\langle \hat{B}^\alpha(x^\alpha, \tau) \hat{B}^{\alpha'}(x^{\alpha'}, 0) \rangle\rangle. \quad \text{(D4)}$$

Performing the quantum average and going to continuous frequencies, one obtains

$$\gamma_\phi^{\alpha\alpha'} = 32\pi (\kappa^\alpha \kappa^{\alpha'})^2 \int d\omega \, N_\omega (1 + N_\omega)$$
$$\times \left[\frac{\omega_{\text{an}}^\alpha \, \omega}{(\omega_{1,0}^\alpha - \omega)(\omega_{2,1}^\alpha - \omega)} \right] \left[\frac{\omega_{\text{an}}^{\alpha'} \, \omega}{(\omega_{1,0}^{\alpha'} - \omega)(\omega_{2,1}^{\alpha'} - \omega)} \right], \quad \text{(D5)}$$

where $N(\omega)$ is the bosonic distribution function. Finally, for similar qubits and a narrow bandwidth $\Delta\omega$ of the transmission line modes, one arrives at the pure dephasing rate

$$\gamma_\phi = 32\pi \kappa^4 \left[\frac{\omega_{\text{an}} \, \omega_0}{(\omega_{1,0} - \omega_0)(\omega_{2,1} - \omega_0)} \right]^2 \Delta\omega \, N_{\omega_0}(1 + N_{\omega_0}). \quad \text{(D6)}$$

2. Qubit relaxation

A lossy transmission line enhances the relaxation time of the qubits through the Purcell effect. The transmission line losses can be accounted for by the dissipator

$$\mathcal{D}_{\text{line}}[\hat{R}] = \gamma_{\text{line}} \left[\sum_n \hat{a}_n \hat{R} \, \hat{a}_n^\dagger - \frac{1}{2} \{ \hat{a}_n^\dagger \hat{a}_n, \hat{R} \} \right] \quad \text{(D7)}$$

in the Lindblad equation for the joint evolution of the density matrix $\hat{R}$ of the full system, qubits, and transmission line,

$$\frac{d\hat{R}}{dt} = -i[\hat{H}, \hat{R}] + \sum_{\alpha=\text{L,R}} \mathcal{D}_{\text{rel}}^\alpha[\hat{R}] + \mathcal{D}_{\text{line}}[\hat{R}], \quad \text{(D8)}$$

with the original Hamiltonian $\hat{H}$ given by Eq. (1), and $\mathcal{D}_{\text{rel}}^\alpha[\hat{R}]$ is a phenomenological dissipator for the qubit α. We perform the unitary transformation $\hat{R} \to \hat{\mathcal{R}} = \hat{U}\hat{R}\hat{U}^\dagger$, with $\hat{U}$ given in Appendix B, that integrates out the transmission line modes in $\hat{H}$ to lowest order. Under this action, the bosonic operators in $\mathcal{D}_{\text{line}}$ are shifted according to

$$\hat{a}_n \to \hat{\mathcal{A}}_n = \hat{U}\hat{a}_n\hat{U}^\dagger \approx \hat{a}_n - [\hat{S}^\dagger, \hat{a}_n]$$
$$= \hat{a}_n + i \sum_{\alpha,i} q_{i,i+1}^\alpha |i\rangle_{\alpha\,\alpha}\langle i+1| \left(\frac{\omega_n}{\hbar C_r} \right)^{1/2}$$
$$\times \frac{\varphi_n^*(x^\alpha)}{\omega_{i+1,i}^\alpha - \omega_n}, \quad \text{(D9)}$$

where $\varphi_n(x) = \cos(\pi n x/\ell)$ and $\varphi_n(x) = i \sin(\pi n x/\ell)$ for even and odd integers n, respectively. The shift includes transitions between qubit levels, and therefore the Lindblad equation for the reduced density matrix $\hat{\rho}(t) = \text{Tr}_{\text{line}}[\hat{R}(t)]$ assumes an additional contribution to the qubit's relaxation due to the decay into the transmission line. Combining Eqs. (D7) and (D9), the decay rate of the qubit is enhanced by the term

$$\gamma_{\text{Pur}}^\alpha = \gamma_{\text{line}} \sum_n \frac{\omega_n}{\hbar C_r} \frac{2|q_{1,0}^\alpha|^2}{(\omega_{1,0}^\alpha - \omega_n)^2} \equiv \sum_n \gamma_{n,\text{Pur}}^\alpha, \quad \text{(D10)}$$

where each partial decay rate $\gamma_{n,\text{Pur}}^{\alpha}$ describes the Purcell decay into a transmission line mode with an index n. Going to the continuum limit $\sum_n \to \int \frac{\ell d\omega}{2\pi v}$, one arrives at

$$\gamma_{\text{Pur}}^{\alpha} = 2\gamma_{\text{line}}(\kappa^{\alpha})^2 \int d\omega \frac{\omega}{\left(\omega_{1,0}^{\alpha} - \omega\right)^2}. \tag{D11}$$

[1] J. C. Maxwell, *Theory of Heat* (Appleton, London, 1871).

[2] K. Maruyama, F. Nori, and V. Vedral, Rev. Mod. Phys. **81**, 1 (2009).

[3] R. Landauer, IBM J. Res. Dev. **5**, 183 (1961).

[4] C. H. Bennett, Stud. Hist. Philos. Mod. Phys. **34**, 501 (2003).

[5] S. Toyabe, T. Sagawa, M. Ueda, E. Muneyuki, and M. Sano, Nat. Phys. **6**, 988 (2010).

[6] J. V. Koski, V. F. Maisi, J. P. Pekola, and D. V. Averin, Proc. Natl. Acad. Sci. (U.S.A.) **111**, 13786 (2014).

[7] J. V. Koski, V. F. Maisi, T. Sagawa, and J. P. Pekola, Phys. Rev. Lett. **113**, 030601 (2014).

[8] E. Roldán, I. A. Martinez, J. M. R. Parrondo, and D. Petrov, Nat. Phys. **10**, 457 (2014).

[9] G. B. Lesovik, A. V. Lebedev, I. A. Sadovskyy, M. V. Suslov, and V. M. Vinokur, Sci. Rep. **6**, 32815 (2016).

[10] A. V. Lebedev, D. Oehri, G. B. Lesovik, and G. Blatter, Phys. Rev. A **94**, 052133 (2016).

[11] N. S. Kirsanov, A. V. Lebedev, I. A. Sadovskyy, M. V. Suslov, V. M. Vinokur, G. Blatter, and G. B. Lesovik, AIP Conf. Proc. **1936**, 020026 (2018); N. S. Kirsanov, A. V. Lebedev, M. V. Suslov, V. M. Vinokur, G. Blatter, and G. B. Lesovik, J. Russ. Laser Res. **39**, 120 (2018).

[12] N. Roch, M. E. Schwartz, F. Motzoi, C. Macklin, R. Vijay, A. W. Eddins, A. N. Korotkov, K. B. Whaley, M. Sarovar, and I. Siddiqi, Phys. Rev. Lett. **112**, 170501 (2014).

[13] N. Leung, Y. Lu, S. Chakram, R. K. Naik, N. Earnest, R. Ma, K. Jacobs, A. N. Cleland, and D. I. Schuster, arXiv:1804.02028.

[14] P. Campagne-Ibarcq, E. Zalys-Geller, A. Narla, S. Shankar, P. Reinhold, L. D. Burkhart, C. J. Axline, W. Pfaff, L. Frunzio, R. J. Schoelkopf, and M. H. Devoret, Phys. Rev. Lett. **120**, 200501 (2018).

[15] B. Hensen, H. Bernien, A. E. Dréau, A. Reiserer, N. Kalb, M. S. Blok, J. Ruitenberg, R. F. L. Vermeulen, R. N. Schouten, C. Abellán, W. Amaya, V. Pruneri, M. W. Mitchell, M. Markham, D. J. Twitchen, D. Elkouss, S. Wehner, T. H. Taminiau, and R. Hanson, Nature (London) **526**, 682 (2015).

[16] P. Kurpiers, P. Magnard, T. Walter, B. Royer, M. Pechal, J. Heinsoo, Y. Salathé, A. Akin, S. Storz, J.-C. Besse, S. Gasparinetti, A. Blais, and A. Wallraff, Nature (London) **558**, 264 (2018).

[17] C. J. Axline, L. D. Burkhart, W. Pfaff, M. Zhang, K. Chou, P. Campagne-Ibarcq, P. Reinhold, L. Frunzio, S. M. Girvin, L. Jiang, M. H. Devoret, and R. J. Schoelkopf, Nat. Phys. **14**, 705 (2018).

[18] S. Lloyd, Phys. Rev. A **56**, 3374 (1997).

[19] J. M. R. Parrondo and J. M. Horowitz, Physics **4**, 13 (2011).

[20] S. W. Kim, T. Sagawa, S. De Liberato, and M. Ueda, Phys. Rev. Lett. **106**, 070401 (2011).

[21] R. Uzdin, A. Levy, and R. Kosloff, Phys. Rev. X **5**, 031044 (2015).

[22] J. M. Horowitz and M. Esposito, Phys. Rev. X **4**, 031015 (2014).

[23] H. T. Quan, Y. D. Wang, Y.-X. Liu, C. P. Sun, and F. Nori, Phys. Rev. Lett. **97**, 180402 (2006).

[24] H. Wang, S. Liu, and J. He, Phys. Rev. E **79**, 041113 (2009).

[25] J. B. Brask, G. Haack, N. Brunner, and M. Huber, New J. Phys. **17**, 113029 (2015).

[26] J. P. Pekola, D. S. Golubev, and D. V. Averin, Phys. Rev. B **93**, 024501 (2016).

[27] P. P. Hofer, M. Perarnau-Llobet, J. B. Brask, R. Silva, M. Huber, and N. Brunner, Phys. Rev. B **94**, 235420 (2016).

[28] M. D. Vidrighin, O. Dahlsten, M. Barbieri, M. S. Kim, V. Vedral, and I. A. Walmsley, Phys. Rev. Lett. **116**, 050401 (2016).

[29] P. A. Camati, J. P. S. Peterson, T. B. Batalhão, K. Micadei, A. M. Souza, R. S. Sarthour, I. S. Oliveira, and R. M. Serra, Phys. Rev. Lett. **117**, 240502 (2016).

[30] N. Cottet, S. Jezouin, L. Bretheau, P. Campagne-Ibarcq, Q. Ficheux, J. Anders, A. Auffèves, R. Azouit, P. Rouchon, and B. Huard, Proc. Natl. Acad. Sci. (U.S.A.) **114**, 7561 (2017).

[31] J. Koch, T. M. Yu, J. Gambetta, A. A. Houck, D. I. Schuster, J. Majer, A. Blais, M. H. Devoret, S. M. Girvin, and R. J. Schoelkopf, Phys. Rev. A **76**, 042319 (2007).

[32] D. M. Pozar, *Microwave Engineering*, 4th ed. (Wiley, Massachusetts, 2012).

[33] C. Y. She, J. Appl. Phys. **36**, 3784 (1965).

[34] J. Majer, J. M. Chow, J. M. Gambetta, J. Koch, B. R. Johnson, J. A. Schreier, L. Frunzio, D. I. Schuster, A. A. Houck, A. Wallraff, A. Blais, M. H. Devoret, S. M. Girvin, and R. J. Schoelkopf, Nat. Lett. **449**, 443 (2007).

[35] N. Schuch and J. Siewert, Phys. Rev. A **67**, 032301 (2003).

[36] N. Khaneja, R. Brockett, and S. J. Glaser, Phys. Rev. A **63**, 032308 (2001).

[37] G. Vidal, K. Hammerer, and J. I. Cirac, Phys. Rev. Lett. **88**, 237902 (2002).

[38] While the SWAP operation replaces product states by product states, the iSWAP gate is entangling in general.

[39] H.-P. Breuer and F. Petruccione, *The Theory of Open Quantum Systems* (Oxford University Press, Oxford, 2003).